Chinese Chemical Letters 35 (2024) 108690

Contents lists available at ScienceDirect

Chinese Chemical Letters

journal homepage: www.elsevier.com/locate/cclet

Efficient photocatalytic NADH regeneration with Rh-loaded Z-scheme mediator-free system

Yi Zhou[a,b,d,*], Yiling He[a,b], Ming Gao[a,b], Ningkai Ding[a], Juying Lei[a,b,c], Yanbo Zhou[a,b,d]

[a] State Environmental Protection Key Laboratory of Environmental Risk Assessment and Control on Chemical Process, East China University of Science and Technology, Shanghai 200237, China
[b] National Engineering Research Center of Industrial Wastewater Detoxication and Resource Recovery, East China University of Science and Technology, Shanghai 200237, China
[c] Shanghai Engineering Research Center for Multi-media Environmental Catalysis and Resource Utilization, East China University of Science and Technology, Shanghai 200237, China
[d] Shanghai Institute of Pollution Control and Ecological Security, Shanghai 200092, China

ARTICLE INFO

Article history:
Received 27 February 2023
Revised 23 May 2023
Accepted 12 June 2023
Available online 22 August 2023

Keywords:
Photocatalysis
NADH regeneration
Mediator-free
Carbon nitride
Z-scheme

ABSTRACT

Nicotinamide adenine dinucleotide (NADH) regeneration is necessary for the sustainable application of enzymatic industry. The Rh-based complex $[Cp^*Rh(bpy)(H)]^+$ has been widely used as an important mediator in NADH regeneration systems, but it is limited by complexity and high cost. Here, a Z-scheme was constructed by loading Rh onto carbon nitride nanosheets/carbon nitride quantum dots (CN-CNQD). The resultant catalyst achieved a high yield of NADH in a mediator-free (M-free) system of 0.283 mmol L^{-1} g^{-1} min^{-1}, which is 5.29 times that of pure CN. ADH enzyme introduction experiments confirmed that the enzyme active product 1,4-NADH could reach 34.21% selectivity in the M-free system. Mechanism research revealed that the heterojunction between CNs and CNQDs improved the NADH regeneration activity in the traditional M-involved system, while Rh loading was proved to optimize the yield and selectivity of 1,4-NADH in M-free system. The immobilized Rh shows more competitiveness than $[Cp^*Rh(bpy)(H)]^+$. This study contributes to the construction of an M-free system for further application in greener, lower-cost enzymatic processes.

Enzymatic reaction has great potential in chemical engineering, energy production and pollution control due to its high efficiency and moderate catalytic environment demand [1–3]. Nicotinamide adenine dinucleotide (NADH) is essential in over 98% of enzymatic reactions as the electron and energy donor, and it is converted into its oxidation form NAD^+ during the process [4]. However, commercial NADH costs over 2600 $/mol [5], making it undesirable to consume NADH as a stoichiometric ingredient in massive production. Thus, the manual NADH regeneration from NAD^+ is significant for further application in the enzymatic industry.

Current attempts for efficient NADH regeneration generally require an organic Rhodium complex $[Cp^*Rh(bpy)(H)]^+$ as the electron mediator (abbreviated as M), which can selectively transfer a hydride to NAD^+ to ensure high regeneration rate and selectivity of the enzymatic active isomer 1,4-NADH [6,7]. Photocatalytic methods have been successfully applied for NADH regeneration under M-involved systems [8]. Zhongyi Jiang *et al.* [9] constructed a Z-scheme heterojunction between g-C_3N_4 and α-Fe_2O_3/C and reached 76.3% NADH formation efficiency in an M-involved system. Chandani Singh *et al.* [10] designed an anthracene-based g-C_3N_4 as a metal-free semiconductor and reached a catalytic efficiency of 76.14% for the NADH formation with M involved. The above researches prove the possibility of manual NADH photocatalytic regeneration with M involved and exhibit the application potential of g-C_3N_4. However, the use of Rh-based mediator brings problems like consumption of rare metals, difficulty in separation [6] and the remaining M in the solution may cause aggregation and deactivation of enzymes, affecting the activity of the following enzymatic process [11]. To solve these problems, few researchers have started the exploration of NADH regeneration under M-free conditions, but usually suffered a considerable performance loss. Yingjie Zhao *et al.* used conjugated COFs as photocatalysts and achieved an extraordinary NADH yield over 74% in 10 min, but received a severely decreased yield of 43.8% under M-free condition [12]. The same result was obtained in another report, in which the fabricated TP-COFs could transform 97% of NAD^+ into NADH under M-involved

* Corresponding author.
E-mail address: yizhou@ecust.edu.cn (Y. Zhou).

https://doi.org/10.1016/j.cclet.2023.108690
1001-8417/

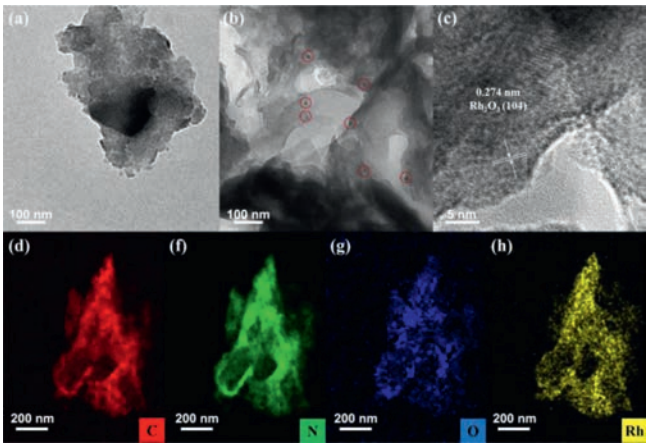

Fig. 1. TEM images (a, b), HRTEM (c) image and element mapping (d-g) of RQCNs.

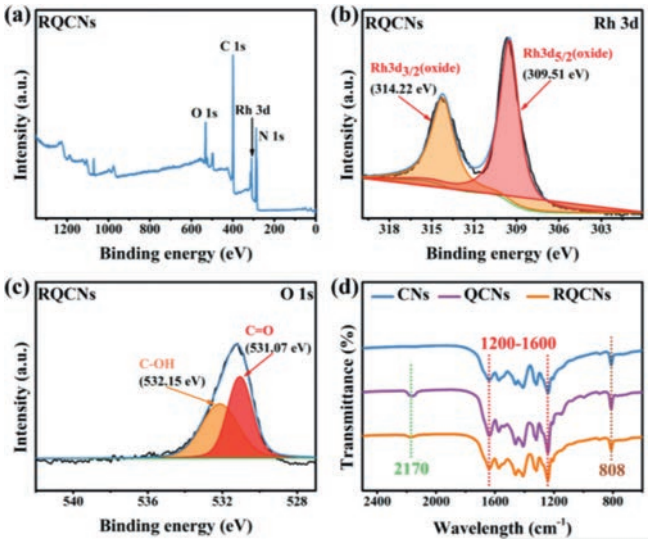

Fig. 2. (a) XPS survey spectra, (b) the Rh 3d XPS spectra, (c) the O 1s XPS spectra and (d) FT-IR spectra of RQCNs.

conditions, but only 45.5% under M-free conditions [13]. Utilizing rhodium (Rh) species in different ways are employed to relieve the performance loss under M-free conditions. Kerstin T. Oppelt *et al.* developed a copolymer with Rh as the active site, which generated only 21% NADH after 26 h of irradiation [14]. Besides, the substitute strategy still suffers from the complicated preparation and high material cost. On the other hand, the interfacial effect of heterojunction could be utilized in NADH regeneration [15,16], but the existence of M, no matter free in the solution or anchored on the catalyst, will inevitably hinder the transmission of electron and proton due to the increased interface. Simplifying the process and loading Rh directly onto the catalyst as a possible active site is a worthwhile attempt [17–20].

Here, we loaded Rh with a simple photo-deposition method onto heterojunctions constructed from carbon nitride (CNs) and carbon nitride quantum dots (CNQDs). CN is a simple semiconductor with no biotoxicity and shares a similar chemical structure with CNQDs, which could help reduce the electron transform resistance [21–23]. Furthermore, Rh was induced as the additional active site to improve the regeneration rate and selectivity of 1,4-NADH. This study focused on the replace of the $[Cp^*Rh(bpy)(H)]^+$ with Rh to construct a photocatalytic NADH regeneration system without mediator participation.

TEM image revealed the nanosheet structure of RQCNs (Fig. 1a). HRTEM images (Figs. 1b and c) illustrated that RQCNs had an apparent lattice of 0.274 nm which can be assigned to the (1 0 4) crystal lattice of Rh_2O_3 (PDF #25-0707) [24]. Element mapping in Figs. 1d-h also confirmed that Rh was uniformly loaded on the nanosheets and energy dispersive spectroscopy (EDS) (Fig. S1 in Supporting information) further measured the actual Rh loading of 7.61% (Table S1 in Supporting information).

XRD patterns of the prepared samples in Fig. S2 (Supporting information) showed the typical diffraction peaks located at ~13.0° and ~27.3°, referring to the (002) and (100) planes of CN, respectively [25]. The results confirmed that the introduction of CNQDs and Rh did not break the original structure of CN. And the peak located at ~27.1° was characteristic of interlayer stacking between conjugated aromatic systems. The intensity of this peak for CNs, QCNs and RQCNs significantly decreased compared with bCN, suggesting their thinner morphology.

XPS was employed to analyze chemical states (Fig. 2 and Fig. S4 in Supporting information). The peaks at 288.18 and 284.60 eV in C 1s spectra (Fig. S3a in Supporting information) were ascribed to C-$(N)_3$, C-C, respectively [26,27]. The peaks at 398.50 and 400.12 eV were ascribed to C-N-C and N-$(C)_3$, respectively (Fig. S3b in Supporting information) [28]. A distinct peak of Rh was observed in the XPS spectra of RQCNs (Fig. 2a, Fig. S4a), indicating the successful loading of Rh. Two distinct peaks located at 309.51 and 314.22 eV are observed in the Rh 3d spectra of RQCNs, attributed to Rh $3d_{5/2}$ and Rh $3d_{3/2}$, indicating Rh is present in the form of Rh_2O_3, consistent with the HRTEM images. (Fig. 2b) [29]. The peak at 531.07 eV in O 1s spectra of RQCNs (Fig. 2c) and the peak at 286.27 eV in C 1s spectra of RQCNs (Fig. S3a) were all assigned to the O-C=O of CNQDs [23,30]. FTIR provided the diffraction peak at 2170 cm^{-1} of QCNs and RQCNs, assigned to the vibration of O-C=O in the CNQDs [31,32]. Those signal peaks were the same as that of QCNs in C 1s (Fig. S4b) and N 1s (Fig. S4c) spectra, confirming the original CN structure was maintained after Rh loading. As shown in Fig. 2d and the enlarged FT-IR spectra in Fig. S5 (Supporting information), all the catalysts remained the characteristic breathing mode of s-triazine units at 808 cm^{-1}, the stretching vibration models of heptazine ring at 1413 cm^{-1}, 1573 cm^{-1} and 1637 cm^{-1}, and the stretching vibration of C-N-C at 1241 cm^{-1} and 1320 cm^{-1} [30,33,34]. The results above validated the successful combination of CNQDs and CNs, together with the loading of oxide Rh_2O_3.

The photocatalytic activities of catalysts were evaluated in both M-involved and M-free NADH regeneration systems. In M-involved systems (Fig. 3a), CNs showed a slight yield improvement than bCN after 120 min irradiation and the photocatalytic regeneration yield increased from 9.29% (bCN) to 35.68% (CNs) due to its enlarged surface area. After coupling with CNQDs, QCNs showed a significantly increased NADH regeneration yield of 71.08% at 90 min. Among the five different photocatalysts, QCNs had the highest reaction rate constant (0.0330 min^{-1}), which was 1.6 times higher than bCN (0.0204 min^{-1}). It further elucidates that CNQDs provides more activate sites for NADH regeneration (Fig. S6a in Supporting information). Further, the introduction of Rh seemed to hinder the regeneration of NADH in the M-involved systems, but the performance of RQCNs (49.21% at 120 min) was still improved compared with CNs. Meanwhile, the absence of CNQDs made the catalytic activity decreased slightly for RCNs. In addition, RCNs (0.0303 min^{-1}) has smaller kinetic constant than RQNs (0.0315 min^{-1}), owing to CNQDs played a greater role in M-involved systems. Compared with CNs (0.0298 min^{-1}), the introduction of Rh can slightly accelerate NADH regeneration in M-involved system (RCNs: 0.0303 min^{-1}). These results showed that CNQDs played a greater role than Rh in M-involved systems. However, the catalysts' performance in M-free systems were totally different. As shown in Fig. 3b, RQCNs maintained the highest yield of 50.53%,

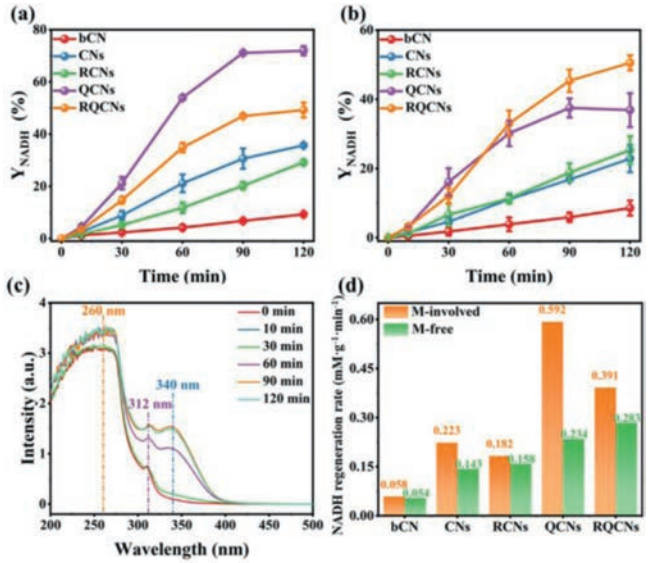

Fig. 3. (a) Yield of NADH with bCN, CNs, RCNs, QCNs and RQCNs in M-involved system; (b) yield of NADH with bCN, CNs, RCNs, QCNs and RQCNs in M-free system; (c) UV-vis spectra of NADH regenerated with QCNs in M-involved system with different irradiation time; (d) initial regeneration rate of NADH with bCN, CNs, RCNs, QCNs and RQCNs in two systems. mM in (d) is mmol/L.

while other samples suffered a decrease in the yield of NADH. And RQNs showed the highest kinetic constant (0.0324 min^{-1}), which is 1.1 times higher than bCN (0.0291 min^{-1}) (Fig. S6b in Supporting information). The performance of QCNs was greatly influenced and dropped to only 36.88%. RCNs showed a higher yield of 25.30% compared with that of CNs (22.88%). From the results above, it was clear that the heterojunction between CNs and CNQDs could improve the regeneration of NADH both in M-involved and M-free systems. The Rh loading may present a negative effect in M-involved system, but the enhancement in M-free system was also significant. The opposite results of Rh species in different reaction system may provide a theoretical possibility to replace M by reasonable catalyst design. From this perspective, we conducted in-depth research of the regenerated products.

UV-vis method is widely used for the measurement of NADH concentration (Fig. 3c). The absorbance peak at 340 nm was ascribed to 1,4-NADH and 1,6-NADH. The peak around 260 nm was ascribed to the common adenine group structure in NAD^+ and NADH. The peak around 312 nm was ascribed to M in the solution [35]. However, UV-vis method could only give an overall concentration of three products at the absorbance of 340 nm, which could not reflect the selectivity of the enzyme-active 1,4-NADH. Thus, ADH enzyme was introduced to validate the 1,4-NADH concentration [35]. As shown in Fig. S7 (Supporting information), ADH enzyme could convert the 1,4-NADH back to NAD^+ during the enzymatic process and lead to an absorbance decrease in the UV-vis spectra, which could represent the actual concentration of regenerated 1,4-NADH. It can be calculated that 94.49% of commercial 1,4-NADH was consumed. Fig. 3d showed the yield and selectivity of 1,4-NADH regenerated by QCNs and RQCNs in different photocatalytic NADH regeneration systems. In M-involved system, 38.48% of the regenerated NADH was the enzyme active 1,4-NADH, which meant that 27.91% of the NAD^+ was converted to 1,4-NADH for QCNs. On the contrary, RQCNs showed a limited yield (19.51%) and selectivity (10.11%) of 1,4-NADH with M involved. In M-free system, the superior performance of QCNs was greatly inhibited, only 6.48% of NAD^+ was converted to 1,4-NADH and the selectivity was only 15.85%. RQCNs showed an increased 1,4-NADH yield of 16.64% and the selectivity was raised to 34.21%. This result proved the positive effect of Rh loading in M-free system, not only the apparent yield of NADH was maintained, more 1,4-NADH was also regenerated during the process. As shown in Fig. S8 (Supporting information), the yield and selectivity of 1,4-NADH at different irradiation time with RQCNs in M-free system was also tested. The yield and selectivity exhibited a synchronous increase and reached the maximum at 120 min. NMR spectra in Fig. S9 (Supporting information) also proved the existence of 1,4-NADH at the chemical shift of 6.8 ppm. ^1H NMR was utilized to estimate the selectivity of the photocatalytic regeneration system for bioactive 1,4-NADH. NAD^+ possesses the characteristic signal at 9.46 ppm [36], whereas after the addition of hydride to the *para*-position of nitrogen cation on the pyridine ring, the characteristic signal of NADH moved to 6.96 ppm [37]. Moreover, some peaks at 8.41 and 8.78 ppm assign to signals of adenosine diphosphate ribose (ADP-ribose) and nicotinamide, respectively [38]. Compared with the performance of QCNs in M-involved system, RQCNs showed a close result of 1,4-NADH regeneration in M-free system, confirming that Rh loading could be considered as a substitute of suspended M in NADH regeneration as expected.

The stability of RQCNs was also investigated and showed in Fig. S10 (Supporting information). After four consecutive cycles, the yield of NADH maintained a good status (Fig. S10a) and the selectivity remained at 29.11% (Fig. S10b). Moreover, QNCs showed a similar loss of activity in the cyclic test (Fig. S10c), which indicated that the loading of Rh is relatively stable. The loss of activity in the cyclic experiment did not originate from the migration of Rh in RQCNs. The slight decrease in catalytic performance was mainly due to the loss during catalyst recovery and some of the active sites of NAD^+ were covered by some fragments generated from excessive oxidation. Furthermore, compared with fresh-made sample, the used RQCNs also maintained the nanosheet structure while the surface is uniformly distributed with Rh nanoparticles (Fig. S11 in Supporting information). It could be attributed to the high stability of RQCNs. NMR spectra in Fig. S12 (Supporting information) confirmed the regeneration of 1,4-NADH at the chemical shift of 6.8 ppm after four cycles. Fig. S13 (Supporting information) showed the XPS spectra of the reused RQCNs. The characteristic peaks of CNQDs and Rh loading were clearly observed, indicating that RQCNs retained good stability after cycle experiments.

Several experiments were performed to explore the possible mechanism for the NADH regeneration process. UV-vis diffuse reflectance spectrometry (UV-vis DRS) was used to investigate the optical properties and band structures of the possible CNs-CNQDs heterojunction catalysts. Fig. 4a showed that all the CN based catalysts got an edge of absorption band at around 450 nm. The bandgap energy (E_g) of all four catalysts are close with the RQCNs exhibiting a relatively wide bandgap of 2.86 eV. As shown in Fig. 4b, the valence band (VB) positions of CNs, QCNs and RQCNs are 2.64, 2.59 and 1.24 eV, respectively. According to $E_{CB} = E_g - E_{VB}$ [39], it can be calculated that the CB of CNs, QCNs and RQCNs are located at−0.07, −0.24 and −1.62 eV, respectively. The most negative conduction band position of RQCNs reveals its maximum potential in NAD^+ reduction. Mott-Schottky was used to evaluate the flat-band potentials of the catalysts (Fig. S14 in Supporting information) and the flat-band potentials of pristine CNs was 0.14 V *vs.* RHE (−0.45 V *vs.* Ag/AgCl), while that of RCNs, QCNs and RQCNs were around 0.13 V *vs.* RHE (−0.46 V *vs.* Ag/AgCl) (Figs. 4c and d). As n-type semiconductors, the flat-band potential will be slightly more positive than the conduction band (CB) potential [40], in agreement with the above calculations. From the above results, it can be speculated that due to the formation of Z-scheme structure, the photoexcited electrons in the CNs' CB would combine holes in the CNQDs' VB, thus the CB position of QCNs and RQCNs shifted to a more negative direction [41], which promoted the NADH regeneration reaction.

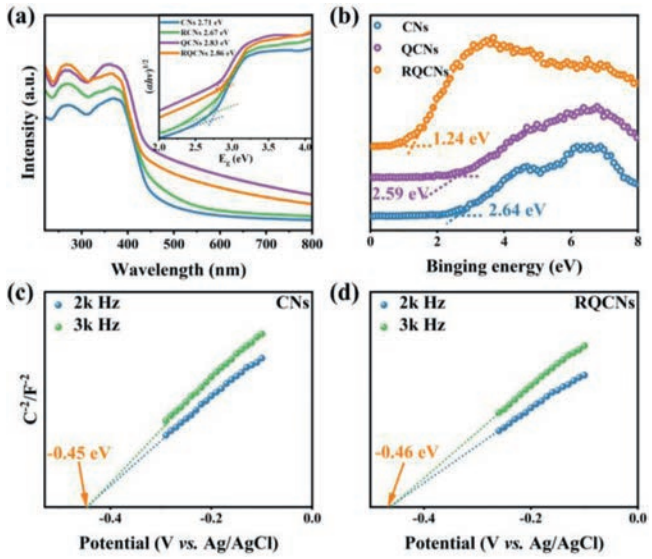

Fig. 4. (a) UV-vis DRS spectra and inset plots of $(\alpha h\upsilon)^{1/2}$ *vs.* photon energy of CNs, RCNs, QCNs and RQCNs; (b) VB XPS spectra of CNs, QCNs and RQCNs; Mott-Schottky plots of (c) CNs and (d) RQCNs.

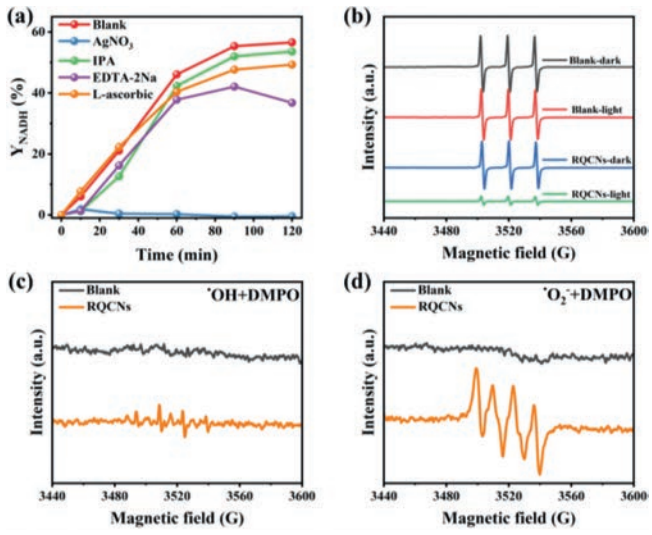

Fig. 5. (a) Free radical capture experiments of RQCNs in M-free system; (b) TEMPO spin-trapping EPR spectra in RQCNs dispersion under visible-light irradiation; DMPO spin-trapping EPR spectra in RQCNs dispersion under visible-light irradiation in aqueous dispersion for DMPO-·OH (c) and in methanol dispersion for DMPO-·O^{2-} (d).

Active species capture experiments and electron paramagnetic resonance (EPR) were used to explore the main active species of the photocatalytic process and verify the possible charge transfer pathways. $AgNO_3$, isopropanol (IPA), ethylenediaminetetraacetic acid disodium salt (EDTA-2Na) and L-ascorbic were used as capture agents for e^-, ·OH, h^+ and ·O^{2-}, respectively. The procedure of free radical capture experiments was introduced in Text S9 (Supporting information). ·OH and ·O^{2-} were detected in the solution. In Fig. 5a, compared with the control group, the capture of e^- would significantly hinder the regeneration of NADH, confirming the dominant effect of e^- in the direct charge transfer from catalysts to NAD^+; the introduction of IPA and L-ascorbic didn't cause much yield loss in the process, indicating that only a small amount of ·OH and ·O^{2-} were produced and contributed little to the regeneration of NADH. However, because the capture agent consumed free radicals and promoted the participation of e^- in free radical production, the amount of e^- involved in NAD^+ reduction was reduced and the activity was slightly lowered [42,43]. As for EDTA-2Na, because the system has added TEOA as h^+ sacrificial agent, its addition caused an excess of sacrificial agent, which further decomposed the already produced NADH and therefore NADH showed a decrease at the last point [44,45]. Fig. 5b showed the EPR results of RQCNs suspension, the signal peak of ·OH and ·O^{2-} can be observed after irradiation (Figs. 5c and d) [46], but the intensity was pretty low, which can was in coincidence with the result of radical capture experiments. Accordingly, the NAD^+ reduction process is shown as reaction equation (Eq. 1):

$$NAD^+ + H^+ + 2e^- \xrightarrow{\text{illumination, catalysts}} NADH \quad (1)$$

To further verify the above results, the photocatalytic NADH regeneration under N_2 atmosphere was carried out. As shown in Fig. S15 (Supporting information), the yield of NADH regeneration under N_2 atmosphere was higher than that of air atmosphere, which can be attributed to the lack of oxygen avoiding competition for electrons, this is consistent with some previous reports [47,48].

Fig. S16 (Supporting information) showed the photoluminescence (PL) emission spectra of different catalysts. It was obvious that the heterojunction and Rh loading could significantly reduce the PL intensity, leading to a lower recombination rate of photoinduced electron-hole. Among all the modified catalysts, RCNs showed the lowest PL intensity, followed by RQCNs. QCNs was the relatively higher one. The results indicated that Rh loading could more effectively suppress the recombination than CNQDs heterojunction. In addition, the blue shift of the PL spectrum indicates that the emission wavelength is shorter and the photon energy required is increased. This further verified that the bandgap width of CNQDs and Rh loaded CNQDs became larger. These results are consisted with that of UV vis-DRS (Fig. 4a). Moreover, compared with CNs, QCNs exhibited a slightly increased photocurrent (Fig. S17 in Supporting information), while RCNs exhibited a remarkably increased photocurrent. Furthermore, the photocurrent intensity of RQCNs was the highest, indicating that the Z-scheme structure had a synergy effect in enhancing the separation and transition efficiency of photoinduced electron-hole.

To study the opposite performance of catalysts in M-involved and M-free systems, room-temperature ns-level time-resolved PL spectra of the catalyst in liquid phase was tested. Fig. S18 (Supporting information) showed the fitting curves of the results, and Table S2 (Supporting information) showed the fitting parameters. For CNs and QCNs, when M was added into the solution, the fluorescence decay times were increased; for Rh loaded samples, however, the fluorescence decay times got decreased after the addition of M. Comparing CNs with QCNs, and RCNs with RQCNs, the CNQDs heterojunction kindly enlarged the influence of M upon the catalysts. The above results indicate that Rh loading has great application potential in the M-free system and can effectively extend the photogenerated carrier lifetime.

Based on the above experimental results and discussion, we propose a mechanism for photocatalytic NADH regeneration in the RQCNs system (Fig. 6). The bandgap structure of CNQDs was obtained from previous reports with CB and VB of −1.09 and 1.45 eV, respectively [49]. Under photoexcitation, e^- in the CB of CNs tend to transfer to the VB of CNQDs through the contact interface, forming a Z-scheme structure. On the CB of CNQDs, NAD^+ combined with e^- for the regeneration of NADH. Besides, Rh loading instead of complex $[Cp^*Rh(bpy)(H)]^+$ is significant in M-free systems.

In summary, a CNs-CNQDs heterojunction with Rh loading catalyst was prepared by solid phase thermal, calcine and photodeposition method. The catalyst was applied for NADH regeneration in a mediator-free system. UV-vis, NMR and ADH enzyme incubation validated its improved yield and selectivity of the enzyme active product 1,4-NADH. Further study proved that the het-

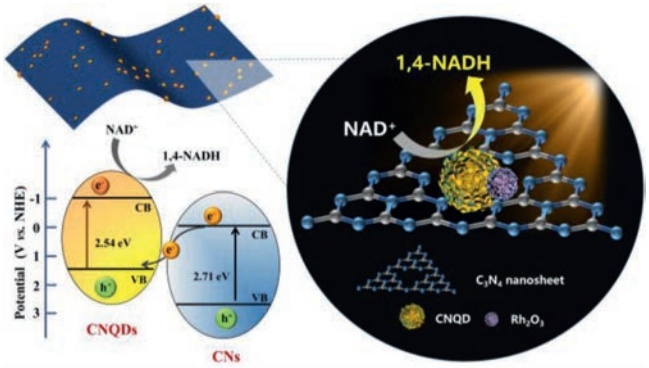

Fig. 6. Mechanism of photocatalytic NADH regeneration for catalysts.

erojunction between CNs and CNQDs could improve the yield of NADH, while Rh loading was the decisive factor that enhanced the selective regeneration of 1,4-NADH in M-free system, and e^- was the dominant active species. This study provided a new method for the development of efficient and economical NADH regeneration in enzyme-catalyst industry.

Declaration of competing interest

There are no conflicts of interest to declare.

Acknowledgments

This work was supported by the National Natural Science Foundation of China (No. 21906056), Open Project of State Key Laboratory of Urban Water Resource and Environment, Harbin Institute of Technology (No. ESK202104), the Science and Technology Commission of Shanghai Municipality (No. 22ZR1418600), Shanghai Municipal Science and Technology (No. 20DZ2250400).

Supplementary materials

Supplementary material associated with this article can be found, in the online version, at doi:10.1016/j.cclet.2023.108690.

References

[1] G. Rehn, A.T. Pedersen, J.M. Woodley, J. Mol. Catal. B: Enzym. 134 (2016) 331–339.
[2] C. Zhang, Y. Tang, Q. Wang, et al., Chin. Chem. Lett. 34 (2023) 107795.
[3] C. Chen, Q. Ma, F. Liu, et al., J. Hazard. Mater. 419 (2021) 126452.
[4] C.S. Morrison, W.B. Armiger, D.R. Dodds, et al., Biotechnol. Adv. 36 (2017) 120–131.
[5] T. Saba, J.W.H. Burnett, J. Li, et al., Chem. Comm. 56 (2020) 1231–1234.
[6] W. Jones, J.W.H. Burnett, J. Shi, et al., Joule 4 (2020) 2055–2059.
[7] J. Liu, X. Ren, C. Li, et al., Appl. Catal. B 310 (2022) 121314.
[8] X. Li, F. Ma, Y. Li, et al., Chem. Eng. J. 389 (2020) 124411.
[9] Y.Z. Wu, J. Ward-Bond, D.L. Li, et al., ACS Catal. 8 (2018) 5664–5674.
[10] C. Singh, T.W. Kim, R.K. Yadav, et al., Int. J. Energy Res. 45 (2021) 13117–13129.
[11] S. Zhang, Y. Zhang, Y. Chen, et al., ACS Catal. 11 (2021) 476–483.
[12] Y. Wang, H. Liu, Q. Pan, et al., J. Am. Chem. Soc. 142 (2020) 5958–5963.
[13] Y. Zhao, H. Liu, C. Wu, et al., Angew. Chem. Int. Ed. 58 (2019) 5376–5381.
[14] K.T. Oppelt, J. Gasiorowski, D.A.M. Egbe, et al., J. Am. Chem. Soc. 136 (2014) 12721–12729.
[15] Y. Zhang, Y. Zhao, R. Li, J. Liu, Solar RRL 5 (2020) 2000339.
[16] Y. Wang, J. Sheng, X. Zhao, et al., Chin. Chem. Lett. 34 (2022) 107967.
[17] H.C. Lo, O. Buriez, J.B. Kerr, R.H. Fish, Angew. Chem. Int. Ed. 38 (1999) 1429–1432.
[18] Y. Maenaka, T. Suenobu, S. Fukuzumi, J. Am. Chem. Soc. 134 (2012) 9417.
[19] Y. Ni, C. Zhou, M. Xing, Y. Zhou, Green Energy Environ (2023), doi:10.1016/j.gee.2023.01.003.
[20] Q. Zeng, S. Chang, M. Wang, et al., Chin. Chem. Lett. 32 (2021) 2212–2216.
[21] Y. He, M. Gao, Y. Zhou, Y. Zhou, Chemosphere 311 (2023) 136925.
[22] Y. Zhou, X. Li, X. Chen, et al., ACS ES&T Water 2 (2022) 2579–2589.
[23] X. Li, J. He, J. Lu, et al., J. Hazard. Mater. 424 (2022) 127650.
[24] K. Maeda, N. Sakamoto, T. Ikeda, et al., Chem. Eur. J. 16 (2010) 7750–7759.
[25] H. Zhao, H. Yu, X. Quan, et al., Appl. Catal. B 152-153 (2014) 46–50.
[26] A.P. Dementjev, A.D. Graaf, D. Van, et al., Diam. Relat. Mater. 9 (2000) 1904–1907.
[27] S.C. Yan, et al., Langmuir 26 (2010) 3894–3901.
[28] S. Yu, R.D. Webster, Z. Yan, X. Yan, Catal. Sci. Technol. 7 (2017) 2050–2056.
[29] A. Gayen, K.R. Priolkar, P.R. Sarode, et al., Chem. Mater. 16 (2004) 2317–2328.
[30] Z. Song, T. Lin, L. Lin, et al., Angew. Chem. Int. Ed. 55 (2016) 2773–2777.
[31] Z. Chen, Y. Wu, Q. Wang, et al., Prog. Nat. Sci. 27 (2017) 333–337.
[32] C. Yang, X. Yu, S. Heißler, et al., Angew. Chem. Int. Ed. 56 (2017) 375–379.
[33] D. Jiang, Q. Xu, S. Meng, et al., J. Alloys Compd. 706 (2017) 41–47.
[34] Y. Yu, W. Yan, X. Wang, et al., Adv. Mater. 30 (2018) 1705060.
[35] J.W.H. Burnett, R.F. Howe, X. Wang, Trends Chem. 2 (2020) 488–492.
[36] J. Liu, M. Antonietti, Energy Environ. Sci. 6 (2013) 1486–1493.
[37] Y. Zhang, Y. Zhao, R. Li, J. Liu, Solar RRL 5 (2021) 2000339.
[38] S. Zhang, J. Shi, Y. Chen, et al., ACS Catal. 10 (2020) 4967–4972.
[39] A. Hankin, F.E. Bedoya-Lora, J.C. Alexander, et al., J. Mater. Chem. A 7 (2019) 26162–26176.
[40] Q. Zhang, Y. Xiao, L. Yang, et al., Chin. Chem. Lett. 34 (2023) 107628.
[41] S. Cheng, Z. Sun, K.H. Lim, et al., Adv. Energy Mater. 12 (2022) 2200389.
[42] L. Xu, J. Wang, Environ. Sci. Technol. 46 (2012) 10145–10153.
[43] Y. Yang, Q. Lai, S. Mahmud, et al., J. Membr. Sci. 645 (2022) 120204.
[44] A. Shi, H. Li, S. Yin, et al., Appl. Catal. B 235 (2018) 197–206.
[45] Ratnawati Slamet, J. Gunlazuardi, E.L. Dewi, Int. J. Hydrog. Energy 42 (2017) 24014–24025.
[46] J. Wang, S. Wang, Chem. Eng. J. 401 (2020) 126158.
[47] H. Wang, J. Chen, Q. Dong, et al., Nano Res. 15 (2022) 5256–5261.
[48] Y. Wu, Y. Chen, D. Li, et al., Appl. Catal. B 309 (2022) 121261.
[49] A. Wang, S. Guo, M. Xu, et al., Appl. Catal. B 322 (2023) 122117.